JACS
JOURNAL OF THE AMERICAN CHEMICAL SOCIETY

ARTICLE

pubs.acs.org/JACS

Anisotropic Organization and Microscopic Manipulation of Self-Assembling Synthetic Porphyrin Microrods That Mimic Chlorosomes: Bacterial Light-Harvesting Systems

Cyril Chappaz-Gillot,[†,▽] Peter L. Marek,[‡,▽] Bruno J. Blaive,[†] Gabriel Canard,[†] Jochen Bürck,[§] Győző Garab,[#] Horst Hahn,[‡,∥,⊥] Tamás Jávorfi,[#] Loránd Kelemen,[#] Ralph Krupke,[‡,⊥] Dennis Mössinger,[‡] Pál Ormos,[#] Chilla Malla Reddy,[‡,⊗] Christian Roussel,[†] Gábor Steinbach,[#] Milán Szabó,[#] Anne S. Ulrich,[§,⊥] Nicolas Vanthuyne,[†] Aravind Vijayaraghavan,[‡] Anita Zupcanova,[#,Δ] and Teodor Silviu Balaban*[,†]

[†]ISM2-Chirosciences, Faculté des Sciences, Aix-Marseille Univ. UMR 6263, Saint-Jérôme, Case A62, Avenue Escadrille Normandie-Niemen, F-13397 Marseille, Cedex 20, France

[‡]Institute for Nanotechnology, [§]Institute for Biological Interfaces, and [⊥]Center for Functional Nanostructures, Karlsruhe Institute of Technology, Postfach 3640, D-76021 Karlsruhe, Germany

[#]Biological Research Center, Hungarian Academy of Sciences, Temesvári körút 62, H-6726 Szeged, Hungary

[∥]Joint Research Laboratory Nanomaterials, Karlsruhe Institute of Technology and Technische Universität Darmstadt, D-64287 Darmstadt, Germany

[Δ]Biological Centre, Academy of Sciences of the Czech Republic, 370 05 Ceské Budejovice, Czech Republic

Supporting Information

ABSTRACT: Being able to control in time and space the positioning, orientation, movement, and sense of rotation of nano- to microscale objects is currently an active research area in nanoscience, having diverse nanotechnological applications. In this paper, we demonstrate unprecedented control and maneuvering of rod-shaped or tubular nanostructures with high aspect ratios which are formed by self-assembling synthetic porphyrins. The self-assembly algorithm, encoded by appended chemical-recognition groups on the periphery of these porphyrins, is the same as the one operating for chlorosomal bacteriochlorophylls (BChl's). Chlorosomes, rod-shaped organelles with relatively long-range molecular order, are the most efficient naturally occurring light-harvesting systems.[1,2] They are used by green photosynthetic bacteria to trap visible and infrared light of minute intensities even at great depths, e.g., 100 m below water surface or in volcanic vents in the absence of solar radiation. In contrast to most other natural light-harvesting systems, the chlorosomal antennae are devoid of a protein scaffold to orient the BChl's; thus, they are an attractive goal for mimicry by synthetic chemists, who are able to engineer more robust chromophores to self-assemble. Functional devices with environmentally friendly chromophores—which should be able to act as photosensitizers within hybrid solar cells, leading to high photon-to-current conversion efficiencies even under low illumination conditions—have yet to be fabricated. The orderly manner in which the BChl's and their synthetic counterparts self-assemble imparts strong diamagnetic and optical anisotropies and flow/shear characteristics to their nanostructured assemblies, allowing them to be manipulated by electrical, magnetic, or tribomechanical forces.

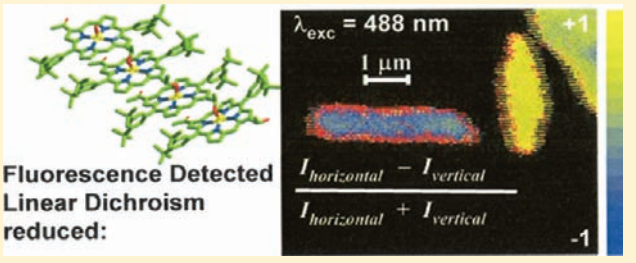

INTRODUCTION

Green photosynthetic bacteria developed some 2.5 billion years ago in an anoxic atmosphere, and they use for light-harvesting special organelles called chlorosomes.[1,2] This name describes their "green sac" nature, as these harbor bacteriochlorophyll (BChl) *c*, *d*, or *e* molecules (Chart 1). In spite of numerous attempts, it has not been possible to obtain single-crystal diffraction data from either chlorosomes or various BChl homologues or derivatives. Solid-state ^{13}C NMR spectroscopy on uniformly labeled samples,[3−6] as well as elegant mutagenesis studies,[7] have demonstrated that these BChl's self-assemble into highly organized extended nanostructures and that proteins, unlike other common photosynthetic antenna systems,[1,2] are not involved in the pigment scaffolding. BChl-containing chlorosomes can scavenge light of minute intensity, such as at 100 m below the water surface[8] or even in volcanic vents at a depth of over 2300 m, where a photosynthetic microbe thrives in the absence of solar radiation by using infrared photons.[9] Once a photon is trapped, one of the BChl molecules becomes excited into the first singlet excited state. Due to the high degree of ordering of the chromophores,[10] the radiant energy is then neatly passed by rapid

Received: May 5, 2011
Published: December 09, 2011

Chart 1. (Top) Chlorosomal BChl's *c*, *d*, and *e* and BChl *a* Encountered in the FMO Complex and within the Baseplate[a] and (Bottom) Zn-C2[b]

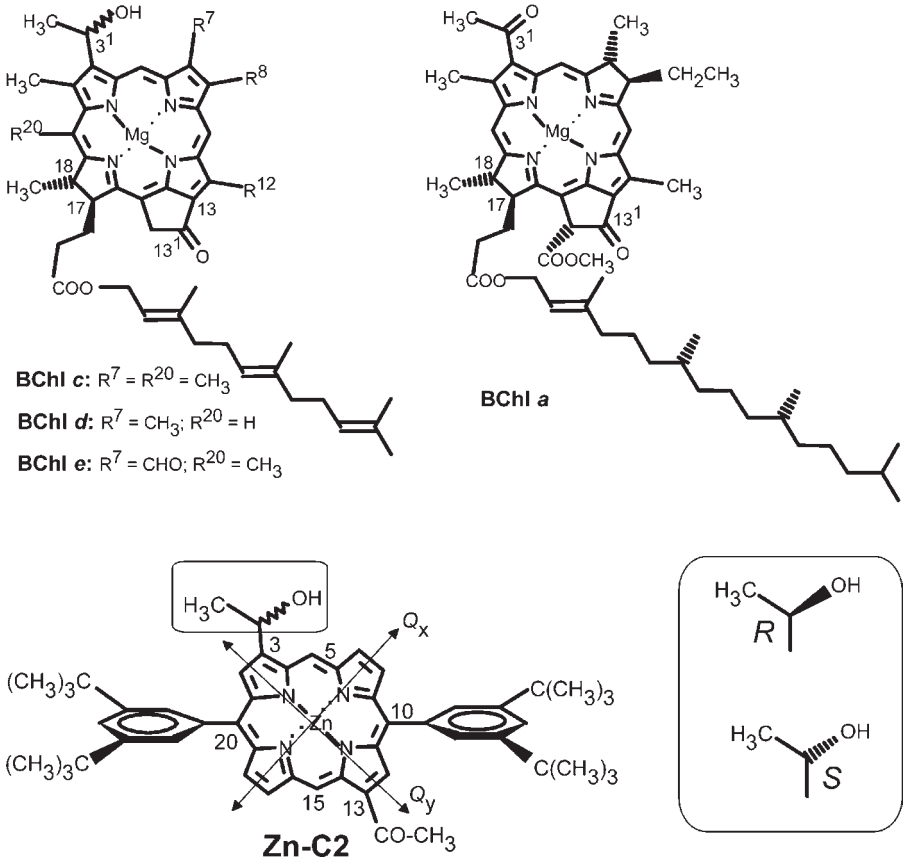

[a] R^8 = ethyl, propyl, or isobutyl (2-methylprop-1-yl); R^{12} = methyl or ethyl. The most common fatty alcohol esterifying the 17-propionic acid residue is shown to be farnesol, but various other alcohols such as phytol (as in BChl *a*), stearol, cetol, and geranyl-geraniol are encountered in different species. [b] **Zn-C2** is the synthetic mimic which self-assembles in nonpolar solvents. The 3-hydroxyethyl substituent (**C2**) can have either handnesses (*R* or *S*), and both are encountered in the chlorosomes. The directions of the $\mathbf{Q}_x$ and $\mathbf{Q}_y$ transition dipole moments are indicated. Longer-chain homologues (**C*n***) have also been prepared.[20,21]

energy-transfer steps to an energetic sink situated in the baseplate of the chlorosome. This energy trap consists of a BChl *a*–protein complex that was actually the very first pigment–protein complex to be characterized by single-crystal X-ray crystallography and is known as the Fenna–Matthews–Olson (FMO) complex.[11] From the FMO complex the excitation energy is transferred to the reaction center, where charge separation occurs, and through a cascade of subsequent electron-transfer steps the hole and the electron become stabilized at opposite sides of the photosynthetic membrane. The reaction center's basic architecture, which is responsible for the directional electron transfer, is common to all photosynthetic organisms. By contrast, there is much variety in antenna systems which are adapted to the habitat's illumination conditions. Ideally, this natural blueprint offered by various biological light-harvesting systems should be technologically reproducible with nonpolluting and nontoxic synthetic pigments capable of photosenzitizing cheap solar cells. We have been able to build self-assembling antenna systems with completely synthetic chromophores in a biomimetic approach.[12−14] A porphyrinoid BChl mimic is shown in Chart 1, and it has the same recognition groups as BChl's *c*, *d*, and *e* appended in the corresponding positions of the macrocycle. We preserve the numbering fashion from BChl's, with the hydroxyalkyl substituent in the northern half and the carbonyl group in the southern half. The central metal ion, which can be either Zn^{2+} or Mg^{2+}, is essential for the self-assembly algorithm to operate, giving similar architectures as judged by various spectroscopic methods.[15] Figure 1 shows typical stationary absorption and fluorescence spectra of monomeric or self-assembled species. Tamiaki[16] and, more recently, Würthner[17] and their co-workers have demonstrated chlorosomal-type self-assembly with semisynthetic molecules derived from chlorophyll *a*. Additionally, Tamiaki has developed elegant multistep syntheses of BChl mimics.[18] Our compounds, being fully synthetic and accessible in only four steps,[19] can be obtained on a larger scale, should applications be envisaged.

The ability to delocalize excitons over large volumes is the main functional feature of the chlorosomal self-assembly. It is indicative of a highly ordered supramolecular chromophore architecture, brought about by ligation of the central metal ion by the hydroxyalkyl and carbonyl substituents. Previously, we have shown that the 3-hydroxyethyl group on a porphyrin framework, present in both types of handedness (i.e., as a racemate), induces the formation of rod-shaped nanostructures, while an achiral 3-hydroxymethyl group leads to the formation of globular self-assemblies.[13] Thus, a single methyl group appended to a porphyrin with a diameter of roughly 1 nm can dictate the shape of

dx.doi.org/10.1021/ja203838p | *J. Am. Chem. Soc.* 2012, 134, 944–954

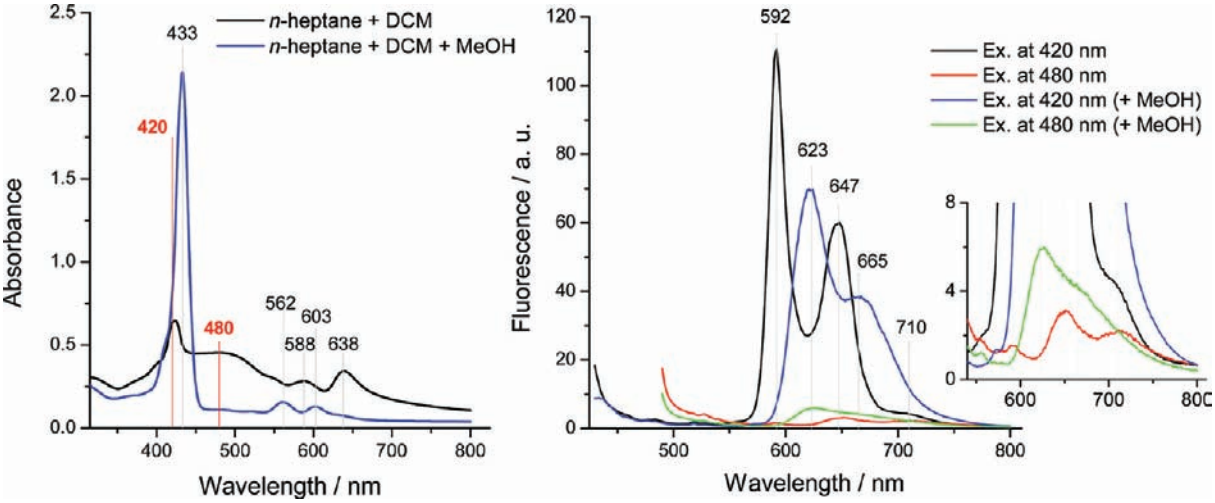

Figure 1. Absorption and fluorescence spectra of **Zn-C2** involved in this study. (Left) Black trace, absorption spectrum of 0.075 mg of (*rac*)-**Zn-C2** dissolved in 10 μL of dry dichloromethane (DCM) which were injected into 1 mL of *n*-heptane; blue trace, after addition of a suprastoichiometric amount of methanol which completely disrupts the self-assemblies. The path length was 5 mm. Numbers indicate absorption maxima in nm. The red vertical lines indicate the two excitation wavelengths at which the fluorescence spectra were measured. (Right) Fluorescence spectra. Inset: magnification of the aggregate-induced fluorescence (red trace) and the monomeric Zn−methanol adduct (green trace), both excited at 480 nm.

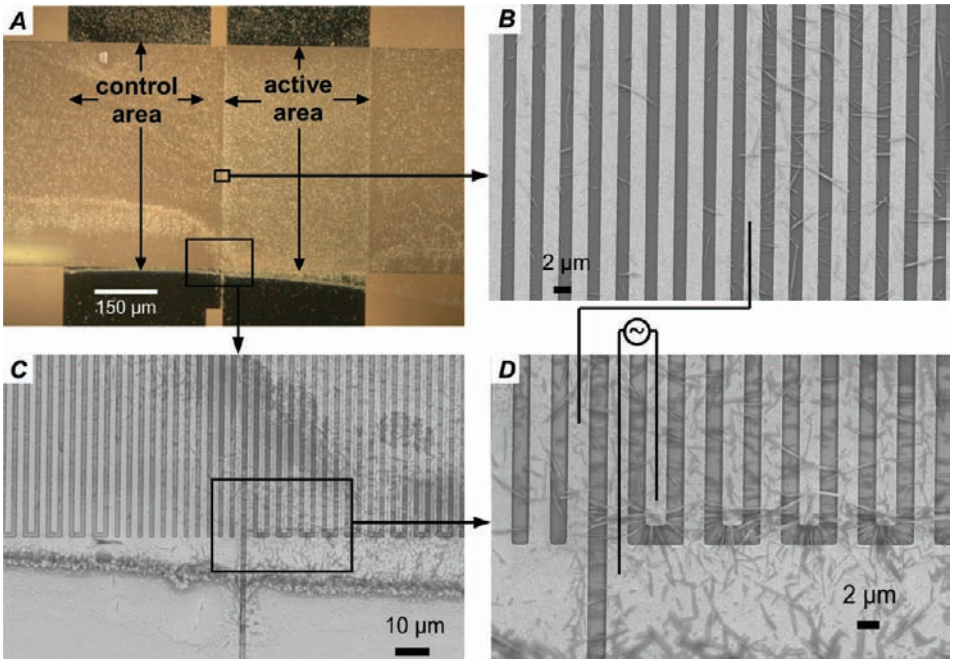

Figure 2. **Zn-C2** aggregates aligned by dielectrophoresis onto an interdigital gold electrode. (A) An optical microscope image which shows the chip with two identical interdigital electrodes (IDEs) on insulating glass, of which only the right one was active, by means of an AC field applied during aggregate deposition. The left one served as a control. The borders of the active area can be seen due to an increased aggregate deposition, having a lighter contrast than the control area. Each of the two IDEs was formed by two gold electrodes on opposing sides (dark areas at the top and the bottom) with interdigitated extensions in between. (B) SEM micrograph of the interface between the active and the nonactive area, (C,D) SEM micrographs of the active electrode in the bottom right corner, imaged in mixed-detector mode (InLens+SE2). On the SEM micrographs the bright areas are the gold layers and the darker ones the glass, which did not charge significantly due to the narrow distance of the conductive gold layers, which were 1.6 μm apart. Panel B shows the alignment of aggregates at the borderline of the active area (right side). Panel C shows the bottom part of the IDE structures, whereas the active area is magnified in panel D. An alternating field of $\pm$80 V at 100 kHz was applied at the active IDE, pulsed at 100 μs with 900 μs pauses to avoid temperature effects due to excessive heating. During the evaporation of ca. 40 μL of a 0.04 mM (*rac*)-**Zn-C2** solution in DCM on the chip, the aggregates were clearly attracted and aligned themselves between the active electrodes, especially at the tips, where the field gradient was maximal.

its self-assembled objects at the micrometer scale. Herein we report other remarkable properties at the macroscale of our prototype molecule **Zn-C2**, which self-assembles into rods or tubules of up to 5 μm length (Supporting Information, Figures S1−S4).

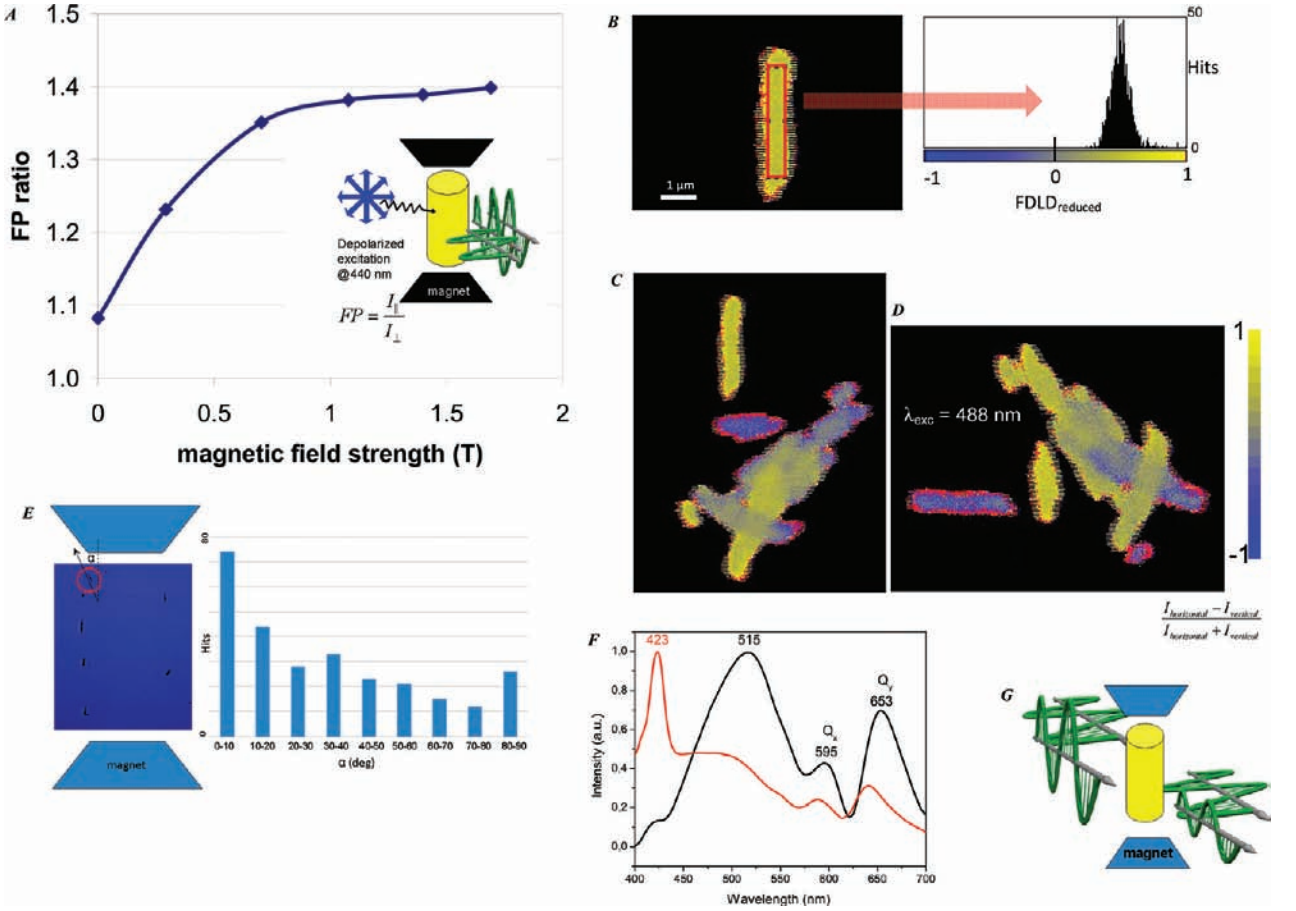

Figure 3. Orientation of **Zn-C2** rods in an external magnetic field and their optical anisotropy. (A) Dependence of the fluorescence polarization ratio of (*rac*)-**Zn-C2** (FP = $I_{\parallel}/I_{\perp}$, i.e., the ratio of the fluorescence intensities of linear polarization parallel with, and perpendicular to, the field vector) on the magnetic field strength. Excitation with depolarized laser beam was at 440 nm, and detection was at >650 nm. (B) Fluorescence-detected linear dichroism (FDLD) normalized to the intensity ($FDLD_{reduced} = (I_v - I_h)/(I_v + I_h)$) of a single rod oriented vertically. The histogram at the right shows the distribution of local FDLD ($= I_v - I_h$) values in the framed area comprising 948 pixels. (C) FDLD showing a conglomerate of tubules sticking together in the absence of a magnetic field. The excitation wavelength was 488 nm, and detection was at >650 nm. (D) Same conglomerate after rotation by 90°. Note the coded color changes which allow the identification of individual tubules within a conglomerate. (E) Optical microscopy image of oriented tubules in a 1.7 T magnetic field. The histogram shows the deviation angle from a collection of 280 objects. The angle of 0° corresponds to the tubules oriented vertically (aligned to the magnetic field), while 90° corresponds to horizontal tubules. (F) Absorption (red trace) and linear dichroism (LD, black trace, scaled arbitrarily) measured in a 0.6 T magnetic field from (*rac*)-**Zn-C2**. The monomer absorption peaks at 423 nm and practically does not contribute to the LD, which originates only from the aggregates' transitions. (G) Pictorial representation of LD = $A_{\parallel} - A_{\perp}$.

Other isomeric mimics with the hydroxyethyl group attached to the 3- or 5-positions and the acetyl group in the 15- or 17-position have been synthesized earlier.[19] Longer alkyl chain homologues **Zn-C*n*** (n = 3−16) have also been synthesized by means of a diacylation reaction followed by statistical monoreduction and zinc insertion.[20,21] This sequence installs hydroxyalkanols in the northern half and acyl moieties with the same number of carbon atoms in the southern half.

RESULTS

Deposition and Orientation of Microrods under Pulsed Dielectrophoretic Conditions. We found that in solution one can grow and deposit the rod-like assemblies of (*rac*)-**Zn-C2** across microelectrodes when these are biased at moderately strong electric fields of 80 V across 1.6 μm ($\sim 5 \times 10^7$ V/m). Figure 2 shows such an interdigitated microelectrode array under an optical microscope (Figure 2A), and within a scanning electron microscope (SEM, Figures 2B−D and S6), at different magnifications and locations. In Figure 2A, the electric field was applied only to opposing electrodes in the right half of the panel, while the left half was unbiased as a control. When a drop of concentrated ($\sim$45 μM), dry dichloromethane (DCM) solution of (*rac*)-**Zn-C2** was placed onto the array, the solvent evaporated rapidly and nanorods—or, rather, microrods—were formed through self-assembly in a process that requires nucleation and resembles crystal growth. Simultaneously, the electric field was applied as 100 μs pulses at 1 ms periods, which translates to 900 μs pauses between pulses, in order to minimize electrothermal heating of the solvent during the deposition process.[22] In the absence of the pulsed field, random aggregation usually occurs as shown in Figures S1−S4, but sometimes "porphyrin wheels" were imaged due to evaporation from DCM microdroplets (Figure S5).[23] Figure 2B−D shows the dielectrophoretic deposition of the aggregates on the biased part of the array, most evident at the corners of the interdigitated electrodes where electrical field gradients are pronounced. To prove that the bridging microrods oriented across the microelectrodes are fully

dx.doi.org/10.1021/ja203838p | J. Am. Chem. Soc. 2012, 134, 944–954

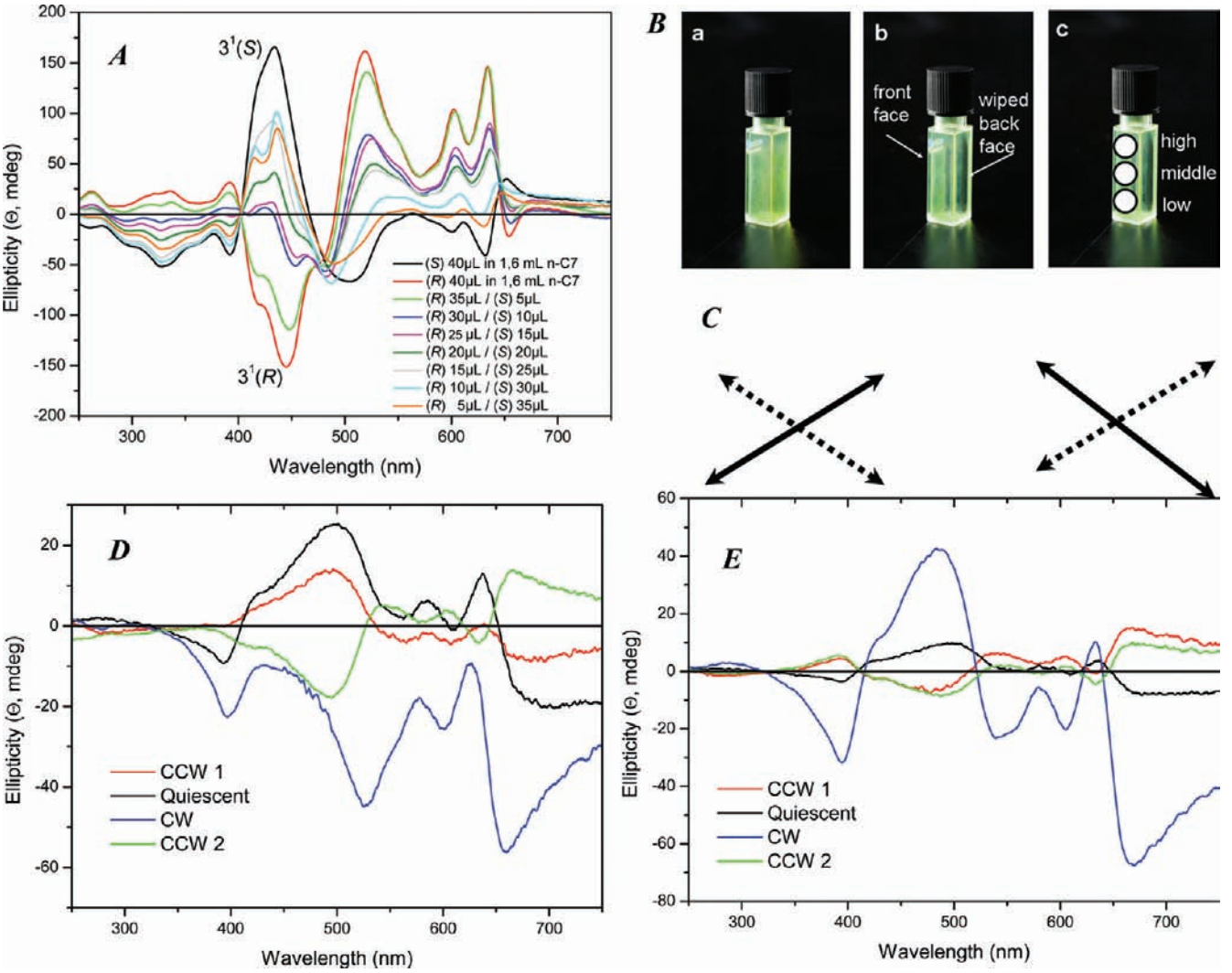

Figure 4. Circular dichroism (CD) spectra. (A) CD traces obtained in solution by titrating different amounts of the 3^1 enantiomers of **Zn-C2** from a 2.4 μmol/mL stock solution in DCM into 1.6 mL of dry *n*-heptane with a path length of 0.5 cm. The top black trace at 450 nm is the enantiopure $3^1(S)$ enantiomer, second eluted, while the bottom red trace is the $3^1(R)$, first eluted. (B) Pictures of the quartz CD cuvette with a thin film before (a) and after (b) wiping clean one face of the cuvette. Different CD/LD spectra are obtained by sampling the film at different heights of the cuvette (c). (C) Directions of the global transition dipole moments on opposite sides of the cuvette when looking from the front face or the back face. (D) CD traces of a quartz cuvette with films on both opposite sides of (*rac*)-**Zn-C2** self-assembled in quiescent *n*-heptane (black trace) or after vortexing for 3 min clockwise (CW, blue trace) or counterclockwise (CCW, red and green traces in two different experiments using the same quartz cuvette and stock solution). In all cases, a 15.5 μmol/L stock solution of (*rac*)-**Zn-C2** in dry DCM was injected in 3 mL of dry *n*-heptane in a rectangular 1×1 cm quartz cuvette which was subsequently vortex stirred. (E) The same experiments as in panel D, but this time the back face of the cuvette was wiped clean. When the square cuvette is rotated by 180°, traces get reversed but are not exactly mirror images, as the distance to the detector is different.

functional as light-harvesting antennas, we illuminated them with monochromatic light and measured the photoconductivity at ±15 V, which shows a relatively fast response for on−off cycles (Figure S7). Some photobleaching eventually occurred after more than 60 min. The gap size between electrodes has a pronounced effect on the deposition tendency, improving toward smaller gaps tested down to 200 nm. Similar depositions could be performed with floating electrodes and the smaller gap sizes, tested in this case down to 400 nm, led to a significantly enhanced aggregate deposition and photoresponse (Figure S8).

Given the high current densities, the porphyrinic self-assemblies seem to be able to withstand rather high temperatures. Their thermal stability was investigated in separate experiments by annealing in an oven at 200 °C. After heating for 15 min, SEM images and absorption spectra showed that the aggregates remained unchanged. Thermogravimetric analysis (Figure S9) proves onset of decomposition above 220 °C. Loss of isobutene from the *tert*-butyl-substituted phenyl groups was demonstrated by coupled mass spectrometry as the major decomposition pathway. A remarkable stability of the self-assemblies was also observed under the electron beam in SEM measurements. Even after 20 min of irradiation, the aggregates remained unchanged. Samples of self-assembled suspensions of (*rac*)-**Zn-C2** had unchanged absorption and fluorescence spectra after more than one year in a sealed cuvette stored on the window pane.

Orientation of the Microrods in a Magnetic Field. For macroscopic handling, dielectrophoresis cannot be readily scaled up. Instead, we were able to orient a much larger amount of

self-assembled (*rac*)-**Zn-C2** in a magnetic field in a simpler fashion. Self-assembly was induced in the adjustable magnetic field within a solenoid coil by injecting a drop (~100 μL) of a concentrated solution in dry DCM (~30 μM) into a much larger volume (typically 3 mL) of dry *n*-heptane. The absorption and fluorescence spectra of these samples are highly indicative of self-assemblies, showing broad and red-shifted maxima, as in J-aggregates[24] (Figures 1 and S11). Addition of solvents that can compete for the central metal ligation (Mg or Zn), such as alcohols or amines, completely disrupts the assemblies into monomeric adducts (Figure 1).

As determined by light microscopy on samples dried in an electromagnet, almost all microrods are aligned parallel with the magnetic field vector. When excited with a depolarized 440 nm laser beam that is absorbed preferentially by the aggregate, the polarized fluorescence emission (FP ratio) shows a marked dependence on the applied magnetic field (Figure 3A). We demonstrate the intrinsic optical anisotropy of the microrods in the absence of any magnetic field by means of Figure 3B, which shows the fluorescence-detected linear dichroism (FDLD) image of a rod recorded in a differential polarization laser scanning–confocal microscope (DP-LSM).[25] This microscope, an LSM equipped with a DP attachment records the FDLD pixel-by-pixel,[26] determines the difference between the absorbances (at 488 nm) associated with two orthogonal polarization states, measured as the difference in the corresponding emission intensities (above 650 nm):

$$\mathrm{FDLD}_{\mathrm{reduced}} = \frac{I_{\mathrm{vertical}} - I_{\mathrm{horizontal}}}{I_{\mathrm{vertical}} + I_{\mathrm{horizontal}}} \qquad (1)$$

Note that the images shown in Figure 3C,D were recorded in the absence of a magnetic field. These experiments demonstrate that the rods exhibit strong anisotropy, which is quite homogeneous along the rod (Figure 3B). Using the microscopic FDLD values, we can calculate that the orientation angle of the absorbance dipoles at 488 nm is about 40° (39° ± 4°) with respect to the long axis of the rod. The strong anisotropic, also quite homogeneous, distribution of the emission dipoles was evinced by imaging the anisotropy, *r*, of the fluorescence emission elicited by depolarized excitation in the DP-LSM,[25] from which the orientation angle of the $\mathbf{Q}_y$ emission dipole could be calculated (37° ± 7°) ($r = I_1 - I_2/I_1 + 2I_2$, with I_1 and I_2 being the polarized emission intensities measured with polarizations parallel with, and perpendicular to, the long axis of the microrod). Linear dichroism (LD) measurements on magnetically aligned macroscopic samples (Figure 4A) show that the orientation angle of the transition dipoles of all main electronic transitions, including the $\mathbf{Q}_x$ (at 588 nm) and $\mathbf{Q}_y$ (638 nm) transitions, are similar to each other, suggesting an east–west orientation of the molecule with respect to the long axis of the rod.

A statistical analysis under the light microscope with an applied magnetic field of 1.7 T yielded the graph in Figure 3E, showing the angular distribution of the main axes of the rods, where $\alpha = 0°$ corresponds to a perfectly aligned microrod. Upon deposition onto clean substrates (Figures S1–S5), in the absence of a magnetic field, the tubules tend to stick to each other with random orientation but their individuality can be clearly discerned by their FDLD or *r*.

We note that thylakoid membranes and grana of green plants show similar albeit somewhat weaker intrinsic fluorescence anisotropies and LD ratios as well as orientation tendencies in external magnetic fields. J-aggregates of *meso*-tetrakis(4-sulfonatophenyl)porphyrin were shown to align in a 10 T magnetic field, forming long tubules oriented with their long axis parallel to the magnetic field.[27] In our case weaker magnetic fields are able to orient the aggregates due to a stronger diamagnetic susceptibility of the extended π-system with push–pull substituents in the 3- and 13-positions, respectively (Figure 1). Recently, whole chlorosomes were imaged at the single molecule level, also showing strong fluorescence polarization (FP) with quite a broad wavelength distribution.[28,29]

Orientation of the Microrods by Turbulent Flows. Flow and shear forces can orient objects with large aspect ratios as is well documented and utilized by microfluidics.[30] Recently, it was shown that one can induce supramolecular helicities in porphyrinic J-aggregates[31−36] and in dendrimeric assemblies by vortex stirring.[37] Complete sign reversals of the resultant intense Cotton effects in circular dichroism (CD) can be achieved by reversing the stirring sense. We subjected the racemic compound (*rac*)-**Zn-C2**, and (*rac*)-**Zn-C7** that has longer alkyl chains and thus experiences more pronounced tribomechanical forces in nonpolar solvents, to vortex stirring. This resulted in the formation of thin films on the cuvette walls, which are discernible to the naked eye (Figures 4D and S11). These films contribute a strong component of LD to the intrinsic CD signal of the molecules (Figures 4B and S10), and this component gets reversed when a fresh suspension is vortexed either clockwise or counterclockwise in the cuvette, as demonstrated in Figure 4E. This orientation by turbulent hydrodynamic flows occurs only for the films, not for the species existing in solution. If a certain critical micellar concentration is surpassed, flocculates form in quiescent cuvettes. These are disrupted by rapid vortexing so that the suspensions appear homogeneous to the eye, mimicking exactly the behavior of the chlorosomal BChl's in nonpolar solvents.[38] Remarkably, neither the film on the cuvette walls, nor the decanted suspensions show by chiral HPLC any enantiomeric enrichment of its components. The racemate is thus microscopically oriented by the shearing forces on the cuvette walls as a 1:1 heterochiral complex. When the same experiment is repeated with the individual enantiomers, film formation and self-assembly is much less pronounced. The respective solutions/suspensions of the $3^1(R)$ enantiomer, first eluted with *n*-hexane/2-propanol (80/20, v/v) from the chiral HPLC column (*S*,*S*)-Whelk and the $3^1(S)$ enantiomer (second eluted) show intense CD signals of opposite signs according to the intrinsic stereochemistry at the 3^1-carbon atom. To demonstrate the 1:1 heterochiral complex formation, a stock DCM solution of the $3^1(R)$ enantiomer was titrated into a DCM solution of the $3^1(S)$ enantiomer. This was then injected into a quiescent excess of *n*-heptane, where it produced a gradual reversal of the CD line shapes, as shown in Figure 4A. Spectra calculated by adding in various proportions the CD spectra of the pure enantiomers gave very similar line shapes to the mixtures. It is noteworthy that the species contributing to intense Cotton effects in solution are the dimers and smaller oligomers, all having different signatures from the larger aggregates and the films. When these enantiomerically pure solutions were vortexed, no significant CD changes were observed upon reversing the stirring direction. However, using enantiomerically enriched mixtures, with which film formation in the quartz cuvette proceeds well, one can again use the vortexing direction to bias the overall helicity of the films that is normally induced in solution only by the intrinsic 3^1-stereocenter. We thus

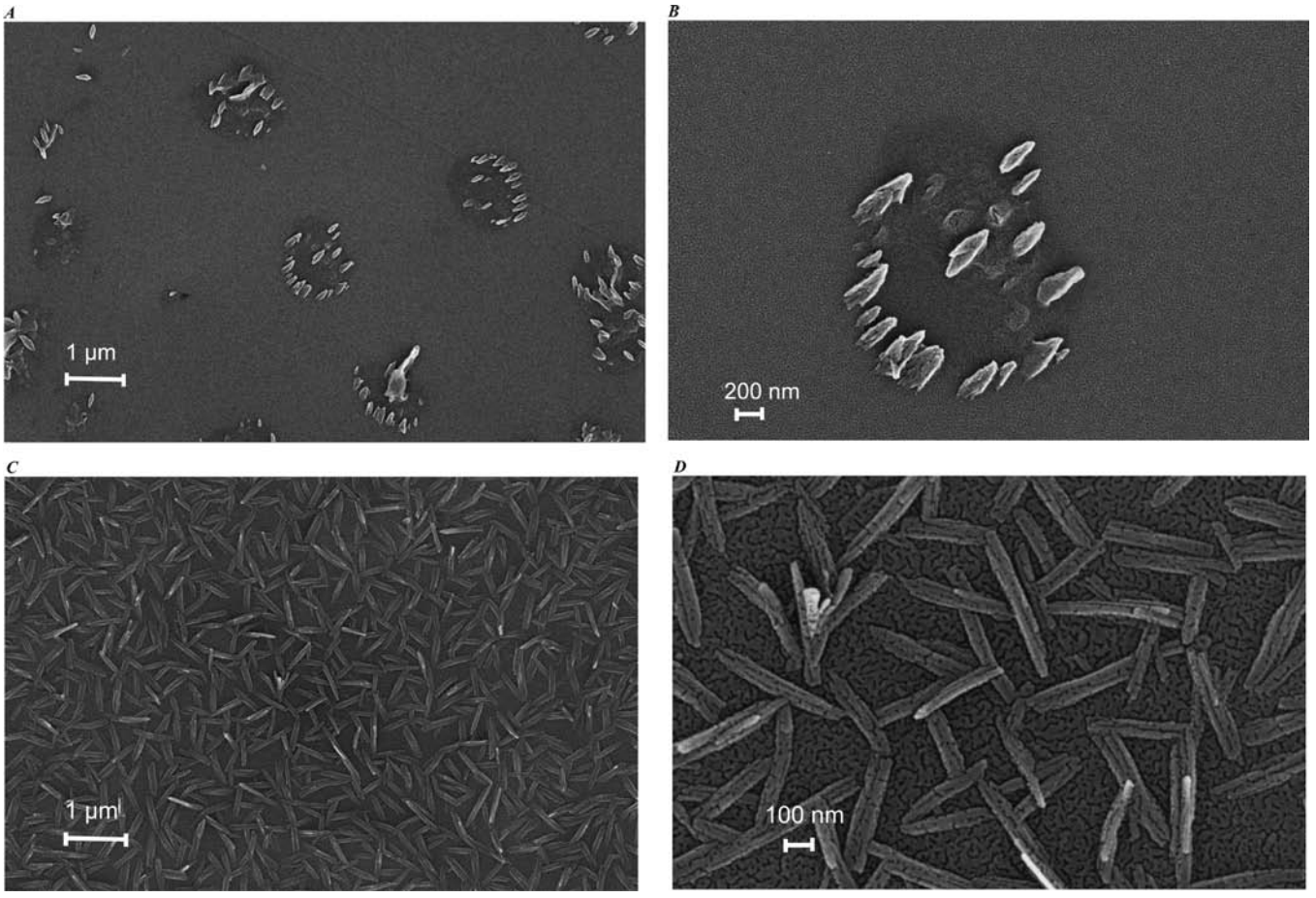

Figure 5. Differences of self-assembled **Zn-C2** onto quartz (A,B) or glass (C,D) substrates imaged by SEM after sputtering with gold. In both cases the films were treated for 4 h. with *n*-heptane at 110 °C.

conclude that the stirring-induced optical dichroism, which it is not active in solution at the molecular level, is a macroscopic effect arising from the self-assembled microrods when they are deposited from the racemate on the quartz cuvette walls as 1:1 complexes. On the walls of glass cuvettes film formation is inhibited, especially if these are heated in an oven at 110 °C prior to the measurements. We presume that adsorbed water on the cuvette walls favors film formation by ligating the Zn atoms.

Initially, we had been rather puzzled that by inducing self-assembly and film formation in quartz cuvettes with racemic samples of **Zn-C2** and **Zn-C7** in quiescent *n*-heptane solutions, some small, nonsilent Cotton effects were observed but with random signs. Apparently, the films deposited on the quartz cuvette walls consist of ordered aggregates, which grow from local nucleation sites of either helical sense when unstirred. Opposing helicities of local domains should cancel statistically when CD or LD spectra are recorded, but any kinetically induced slight excess must have led to the weak residual signals observed. Upon stirring, self-assembly of the films appears to occur with only one preferred helical sense. In the subsequent vortexing experiments we therefore wiped clean one inner face of the quartz cuvette and recorded CD spectra from the film remaining on the opposite face, which gave reproducible results (Figure 4E,F). The helicity of the self-assemblies was thus induced only by the vortexing direction. We noted, however, some variations depending on the height at which the cuvette wall was examined. One possible explanation is that, on quartz, preferential macrodomains are formed and these contribute differently to the CD/LD signals. Support for this hypothesis came from SEM images of films of (*rac*)-**Zn-C2** that were treated with boiling *n*-heptane at 110 °C for four hours. On a quartz substrate clear islands are visible, with the rods sitting in an upright orientation (Figure 5A,B), while on glass the very uniformly sized rods arrange in a random orientation and lie flat on the surface when this is in contact with the solvent vapor (Figure 5C,D).

There is a large contribution to the CD signal stemming from LD (Figure S10). When the rectangular cuvette is turned by 90° or 180°, that is when the beam direction to the film is reversed, the LD signals were sometimes inverted. This is probably due to the fact that the beam of light samples different regions. In order to record oriented circular dichroism (OCD) spectra of (*rac*)-**Zn-C2** on quartz discs, we removed the LD effects by rotating the sample at several different angles around the beam axis and averaging the spectra. LD and OCD curves are shown in Figures S10 and S12, respectively. Again, when the self-assembly was allowed to occur from quiescent *n*-heptane, the $3^1(R)$ and $3^1(S)$ enantiomers showed Cotton effects of opposite signs, while in this case the racemate gave a perfectly silent OCD curve.

Ribó and co-workers have recently summarized the caveats associated with measuring CD signals of supramolecular species built from achiral building blocks.[34] Besides the need to subtract contributions from birefringence and LD components,

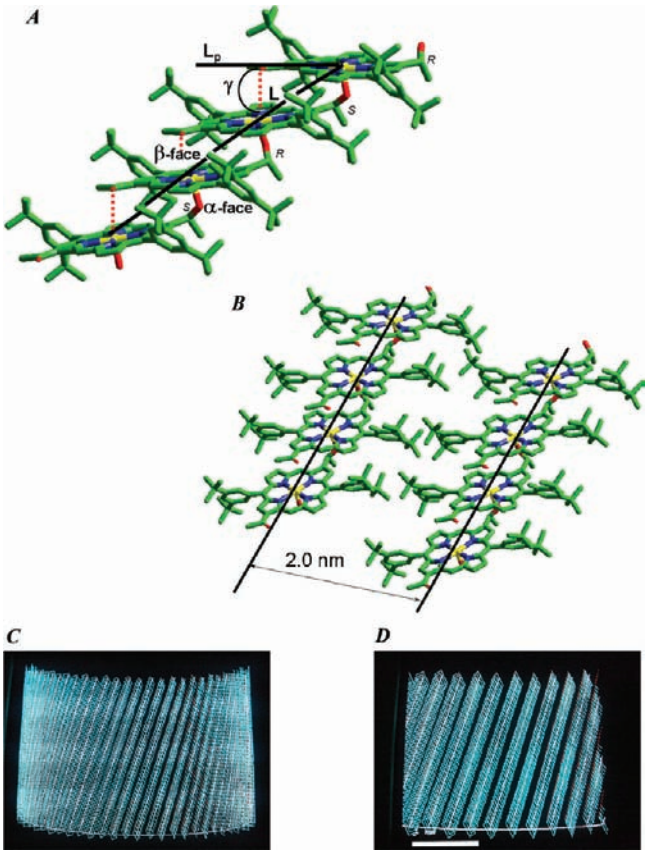

Figure 6. Model of self-assembled tubules from (*rac*)-**Zn-C2**. (A) A stack represented by four **Zn-C2** molecules showing the definition of the angle γ formed by the line **L** joining the Zn^{2+} ions and its projection, $\mathbf{L_p}$, onto the median porphyrin plane. Note the strong Zn−OH ligation on the α−side and weak Zn···O=C< interactions (dotted red lines shown for only three molecules) on the β−side, assuring a 5 1/2 coordination of the zinc ion. (B) Two parallel running stacks with 2.0 nm spacings between the Zn^{2+} ions (yellow). Carbon atoms are green, nitrogen atoms are blue, and oxygen atoms are red. (C) View of the front face of a tubule where the tetrapyrrolic macrocycle is represented by a parallelogram. (D) Enlargement showing parallel running stacks. The scale bar is 10 nm.

which is nontrivial with commercial spectrometers,[39] the effects of vortexing have to be taken into account. In the usual rectangular cuvettes, the inner descending vortex is opposed by chaotic counter-vortices at the four corners. In cylindrical cuvettes, the chiral flows are opposed in the center and near the walls.[35] When film deposition is observed,[36] this can have opposite CD and LD signals to the aggregated species existing in solution. Finally, the vortex generation is complicated because mechanical stirrers or rotary evaporators usually cannot easily be reversed. Even gravity and centrifugal forces can act on the scale of the macroaggregates, and these may contribute differently in the case of clockwise or counter-clockwise vortexing. We found that a small magnetic stirring bar at the bottom of the rectangular 1×1 cm quartz cuvette is not sufficient to bias chiral film formation even after prolonged stirring for 1 h. However, three minutes of intense vortexing using an excentrical rotary stage produces films giving strong circular and linear dichroic signals depending on the vortexing direction—which may be reversed by holding upside down the rotary stage as shown in Figure S11. The present study may suffer from some of these drawbacks; nevertheless, trends are clearly visible and these will be investigated further with custom-built equipment.

DISCUSSION

Despite numerous attempts, we have been unable to solve crystal structures from (*rac*)-**Zn-C2** or its magnesium analog (*rac*)-**Mg-C2**. In the few cases that yielded well formed crystals, these diffracted weakly even on the ANKA Synchrotron and gave poor data sets. We have, however, solved the single crystal structures of several closely related analogs of (*rac*)-**Zn-C2**, namely those with the same *rac*-1-hydroxyethyl and acetyl recognition groups appended to the *meso*-5,15-positions, respectively,[13] and those with identical 3- and 13-acetyl substitutents.[14c] Ligation of the Zn ion by the hydroxyethyl substituent is complemented by a weak electrostatic interaction on the opposite side of the tetrapyrrole with a weak >C=O···Zn interaction, ensuring a 5 1/2 coordination of the central metal ion.[12,40] These interactions between the recognition groups and the Zn^{2+} ion are reinforced by $\pi-\pi$ interactions between the macrocycles which "stack" with an offset and an approximate 3.3 Å interplanar distance. Figure S13 depicts a tetramer issued from such a stack. Identical "staircase architectures" were obtained by Lindsey et coll.[41] for similar porphyrins but with different recognition groups. It appears, therefore, that a general packing motif seems to operate in all these cases. We thus combined small-angle X-ray scattering (SAXS) data with HR-TEM images from various isomers of (*rac*)-**Zn-C2**, including the ones of which single crystal X-ray data were available, in order to generate a three-dimensional molecular model, as illustrated in Figure 6. This assembly produces sharp reflexes in the Fourier transform images corresponding to a ∼2 nm distance and parallel striations running along the long axis of the microrods (Figure S14).[13]

Pšenčik et al.[42] have investigated native chlorosomes from various bacteria by SAXS and cryo-HR-TEM and found similar 2 nm regular spacings, which they interpreted as a lamellar model for the chlorosomal architecture. More recently, the groups of de Groot, Holzwarth, and Bryant carried out an in-depth investigation on a mutant expressing only one type of BChl *d*.[6] By combining cryo-HR-TEM with distance constraints obtained from solid-state NMR with molecular modeling, they proposed a concentric model with several layers of BChl's coordinated from one or the other of the nonequivalent sides.[6] Presently, there is consensus that the architecture of natural chlorosomes suffers from considerable disorder and that frequent "defects" alter an otherwise monotonous structure.[29] In the crystal structure of the 5-hydroxyethyl-15-acetyl isomer of (*rac*)-**Zn-C2**, the hydroxyethyl substituent is disordered over two preferential positions corresponding to both enantiomers.[13] It is thus presently not possible to discern if the stacks are homo- or heterochiral. With the separated enantiomers, as judged from the absorption and CD spectra, homochiral stack formation occurs but (S)TEM and AFM images show that tubules and microrod formation is hindered. It is probable that the hydrophobic 3,5-di-*tert*-butylphenyl groups ensure the microrod formation and this is thermodynamically favored only for heterochiral assemblies.

In our synthetic mimics the rods imaged by HR-(S)TEM appear to be flat, but this could result from collapse of a tubule under the high vacuum conditions. We thus have to leave open the question as to whether the tubules are hollow or consist of concentric rolls. The parallel streaks (ridges, grooves) that run

dx.doi.org/10.1021/ja203838p | *J. Am. Chem. Soc.* 2012, 134, 944–954

nearly parallel with the rod axis, could correspond to helices with a very large pitch. Assuming that the contrast in HR-TEM images must arise from Zn^{2+} ions or overlapping carbon atoms, as if the macrocycles were imaged edge-on, we constructed a crude three-dimensional model to explain both the overall architecture and its apparent inhomogeneity; as illustrated in Figure 6. In Figure 6A we have represented a tetramer composed of both $3^1(R)$ and $3^1(S)$ enantiomers. In Figure 6B two parallel running stacks are shown with 2.0 nm Zn−Zn distances between them. Furthermore, the orientations of the transition dipole moments match those determined by the anisotropy measurements in the magnetic field. Thus, an angle γ of 30° is determined between the line, **L**, joining the metal ions and the tetrapyrrole, which is assumed to be planar ($\mathbf{L_p}$).

The relatively long-range order of the chromophores is essential for light-harvesting so that excitons can diffuse over long distances. Misplaced components can arise due to a change in the coordination of the Zn^{2+} ion from one side (α, anti) or the other (β, syn).[43−47] This inhomogeneity may partially explain the poor crystallization tendency. Nevertheless, this model, which is detailed in the Supporting Information, accounts for the various macroscopic properties described above.

CONCLUSIONS

The tubular microrods formed by self-assembling BChl mimics can be manipulated at the macroscopic level using electrical, magnetic, and tribomechanical fields, and they can be moved or rotated along their long axes in either direction by a laser-optical tweezer.[48] The microrods suspended in viscous *n*-decane at room temperature can steadily be grabbed by optical tweezers. The rods orient themselves with their long axes along the beam, as expected.[48] When the trapping laser is turned off transiently, these tubes are freed, but they can easily be recaptured. The Supporting Information shows short videos of a tubule imaged with an optical microscope. Such degree of control over self-assembled chromophores at the nano- to microscale is unprecedented, to our knowledge. Other densely packed chromophores, such as J-aggregates[24,49] or even hemozoin used by various malaria-causing insects to detoxify iron-rich β-haematin assemblies,[50,51] may well exhibit similar features. These ensemble properties, which are also present, to a lesser extent, in natural chloroplasts,[52] must thus originate from the long-range order of the chromophore dipole moments. Undoubtedly, this feature is essential for the light-harvesting function in natural antenna systems. Replicating these with artificial chromophores is challenging but is certainly worth pursuing with a view to obtain efficient, robust, and cheap solar cells that can function also under dim light.[53] Improving the light-harvesting ability by reaching into the near-infrared region with self-assembling chromophores such as phthalocyanines appears possible and is currently being optimized in our laboratories.

EXPERIMENTAL SECTION

Detailed synthetic procedures for the preparation of the ketols **Zn-C2** and **Zn-C7** are given elsewhere.[20] Stirring experiments were performed with either an Electronic Stirrer Model 300 from Rank Brothers Ltd. (Cambridge, UK), which can stir remotely a magnetic bar with up to 1800 rpm both clockwise (CW) and counter-clockwise (CCW), or alternatively with an excentric stirring plate Vortex Genie 2 from Scientific Industries, (New York, NY), capable of CCW stirring in the normal position or CW when held upside-down (Figure S11).

Fluorescence Polarization Measurements. FP was measured on a home-built instrument as a function of the magnetic field strength of 0−1.7 T in the horizontal (x) direction. The excitation was provided, in the vertical (z) direction, with the depolarized beam of a 440 nm diode laser (Coherent). The fluorescence was observed from the front side of the cuvette in a direction (y) perpendicular to the magnetic field vector. The photomultiplier was protected against the stray light of excitation by a cutoff filter (>650 nm). FP of the emission components parallel with, and perpendicular to, the magnetic field vector was determined with the aid of a Polaroid sheet that was rotated between positions transmitting in the z and x directions, respectively.

Anisotropy (r) of the fluorescence emission carries information on the orientation of the emission dipoles with respect to the long axis of the rods:

$$r = \frac{I_1 - I_2}{I_1 + 2I_2}$$

The depolarized laser beam excites the absorbing dipoles without photoselection; the polarized fluorescence emission carries information on the spatial distribution of the emitting dipoles. Nonpolarized excitation was at 488 nm; polarized emissions are I_1 for vertically and I_2 for horizontally polarized fluorescence.

Linear Dichroism. LD was measured as the difference between the absorbances of horizontally and vertically polarized beams ($LD = A_{\parallel} - A_{\perp}$) in a Jobin Yvon CD 6 dichrograph equipped with an additional board that modulated the polarization state of the measuring light between horizontal and vertical polarizations. A freshly prepared sample, in a 0.5 cm wide glass cuvette with an optical path length of 1 cm, was oriented with the aid of a pair of permanent magnets (0.6 T). Subscripts $\parallel$ and $\perp$ respectively stand for the directions parallel and perpendicular to the magnetic field vector (and also to the preferential orientation of the rods).

Circular Dichroism. CD spectra were measured in rectangular quartz (Suprasil) cuvettes with 1 cm path length from Hellma on JASCO 815 spectrometers in Karlsruhe and Marseille. Spectra were measured in the same cuvette, always in the same orientation, and were baseline subtracted. Oriented CD spectra were measured on a JASCO 810 spectrometer equipped with a home-built sample holder which allows rotation of the solid sample deposited as a film on quartz discs.[54]

ASSOCIATED CONTENT

Supporting Information. SEM images of (*rac*)-**Zn-C2** aggregates on various substrates in the absence of magnetic or electrical fields; size-selective separation of the tubular aggregates under dielectrophoretic conditions; photoconductivity measurements on (*rac*)-**Zn-C2** aggregates; deposition of (*rac*)-**Zn-C2** aggregates between floating electrodes; thermogravimetric analysis of (*rac*)-**Zn-C2** coupled with mass spectrometry; LD and CD spectra of (*rac*)-**Zn-C2**; LD of the separated enantiomers of **Zn-C2**; absorption and CD spectra of (*rac*)-**Zn-C2**; OCD spectra of the separated enantiomers of **Zn-C2**; a tetramer of the 3,13-diacetyl analogue of **Zn-C2** in the crystal; bright-field TEM micrograph of (*rac*)-**Zn-C2** aggregates; model for the self-assembly of chlorosomal BChl mimics; complete ref 20; and videos of a tubule under the light microscope captured by laser tweezers. This material is available free of charge via the Internet at http://pubs.acs.org.

AUTHOR INFORMATION

Corresponding Author
ts.balaban@univ-cezanne.fr

Present Addresses
[⊗]Indian Institute of Science Education and Research, Kolkata, West Bengal, India

Author Contributions

▽These authors contributed equally to this work.

■ ACKNOWLEDGMENT

Michel Cadilhac is thanked for his advice regarding the modeling of the tubules and John A. Berriman for helpful discussions regarding the HR-(S)TEM images. The reviewers have contributed valuable suggestions that are gratefully acknowledged. Roger B. Mallion kindly provided expert help with the manuscript. Partial financial support was granted by the Deutsche Forschungsgemeinschaft through the Center for Functional Nanostructures at the Universität Karlsruhe (Projects C3.5 and C3.5b to S.T.B., E1.2 to A.S.U.). The collaborative work between Marseille and Karlsruhe was facilitated by the CNRS through PICS No. 3777 allocated to C.R. Funding from the Initiative and Networking Fund of the Helmholtz-Gemeinschaft Deutscher Forschungszentren (VH-NG-126) is acknowledged by R.K. and A.V. This work was in part supported by the Hungarian Scientific Research Fund (OTKA/NKTH CNK 80345 to G.G., GOP-1.1.2-07/1-2008-0007 to G.S. who thanks Biofotonika R&D Ltd. for additional funding).

■ REFERENCES

(1) Blankenship, R. E. *Molecular Mechanisms of Photosynthesis*: Blackwell: Oxford, 2002.

(2) Frigaard, N. U.; Bryant, D. A. Chlorosomes: Antenna organelles in photosynthetic green bacteria. In *Microbiology Monographs: Complex Intracellular Structures in Prokaryotes*; Shively, J. M., Ed.; Springer: Berlin, 2006; Vol. 2, pp 79−114.

(3) Nozawa, T.; Ohtomo, K.; Suzuki, M.; Nakagawa, H.; Shikama, Y.; Konami, H.; Wang, Z.-Y. *Photosynth. Res.* **1994**, *41*, 211–223.

(4) Balaban, T. S.; Holzwarth, A. R.; Schaffner, K.; Boender, G.-J.; de Groot, H. J. M. *Biochemistry* **1995**, *34*, 15259–15266.

(5) Kakitani, Y.; Koyama, Y.; Shimoikeda, Y.; Nakai, T.; Utsumi, H.; Shimizu, T.; Nagae, H. *Biochemistry* **2009**, *48*, 74–86.

(6) Ganapathy, S.; Oostergetel, G. T.; Wawrzyniak, P. K.; Reus, M.; Gomez Maqueo Chew, A.; Buda, F.; Boekema, E. J.; Bryant, D. A.; Holzwarth, A. R.; de Groot, H. J. M. *Proc. Natl. Acad. Sci. U.S.A.* **2009**, *106*, 8525–8530.

(7) Frigaard, N.-U.; Gomez Maqueo Chew, A.; Li, H.; Maresca, J. A.; Bryant, D. A. *Photosynth. Res.* **2003**, *78*, 93–117.

(8) Manske, A. K.; Glaeser, J.; Kuypers, M. M. M.; Overmann, J. *Appl. Environ. Microbiol.* **2005**, *71*, 8049–8060.

(9) Beatty, J. T.; Overmann, J.; Lince, M. T.; Manske, A. K.; Lang, A. S.; Blankenship, R. E.; Van Dover, C. L.; Martison, T. A.; Plumley, F. G. *Proc. Natl. Acad. Sci. U.S.A.* **2005**, *102*, 9306–9310.

(10) Fetisova, Z. G.; Freiberg, A. M.; Timpmann, K. E. *Nature* **1988**, *334*, 633–634.

(11) Fenna, R. E.; Mathews, B. W. *Nature* **1975**, *258*, 573–577.

(12) Balaban, T. S. *Acc. Chem. Res.* **2005**, *38*, 612–623.

(13) Balaban, T. S.; Linke-Schaetzel, M.; Bhise, A. D.; Vanthuyne, N.; Roussel, C.; Anson, C. E.; Buth, G.; Eichhofer, A.; Foster, K.; Garab, G.; Gliemann, H.; Goddard, R.; Javorfi, T.; Powell, A. K.; Rosner, H.; Schimmel, T. *Chem.—Eur. J.* **2005**, *11*, 2268–2275.

(14) (a) Huijser, A.; Marek, P. L.; Savenije, T. J.; Siebbeles, L. D. A.; Scherer, T.; Hauschild, R.; Szmytkowski, J.; Kalt, H.; Hahn, H.; Balaban, T. S. *J. Phys. Chem. C* **2007**, *111*, 11726–11733. (b) Balaban, M. C.; Balaban, T. S. *J. Porph. Phthal.* **2007**, *9*, 277–286. (c) Jochum, T.; Reddy, C. M.; Eichhofer, A.; Buth, G.; Szmytkowski, J.; Kalt, H.; Moss, D.; Balaban, T. S. *Proc. Natl. Acad. Sci. U.S.A.* **2008**, *105*, 12736–12741.

(15) (a) Bystrova, M. I.; Mal'gosheva, I. N.; Krasnovskii, A. A. *Mol. Biol.* **1979**, *13*, 440–451. (b) Smith, K. M.; Kehres, L. A.; Fajer, J. *J. Am. Chem. Soc.* **1983**, *105*, 1387–1389. (c) Brune, D. C.; Nozawa, T.; Blankenship, R. E. *Biochemistry* **1987**, *26*, 8644–8652. (d) Brune, D. C.; King, G. H.; Blankenship, R. E. *Photosynthetic light-harvesting systems*; Walter de Gruyter: Berlin, 1988; pp 141−151.

(16) (a) Tamiaki, H.; Takeuchi, S.; Tanikaga, R.; Balaban, S. T.; Holzwarth, A. R.; Schaffner, K. *Chem. Lett.* **1994**, 401–402. (b) Tamiaki, H.; Amakawa, M.; Shimono, Y.; Tanikaga, R.; Holzwarth, A. R.; Schaffner, K. *Photochem. Photobiol.* **1996**, *63*, 92–99. (c) Tamiaki, H.; Miyatake, T.; Tanikaga, R.; Holzwarth, A. R.; Schaffner, K. *Angew. Chem., Int. Ed. Engl.* **1996**, *35*, 772–774. (d) Tamiaki, H.; Amakawa, M.; Shimono, Y.; Tanikaga, R.; Holzwarth, A. R.; Schaffner, K. *Photochem. Photobiol.* **1996**, *63*, 92–99. (e) Tamiaki, H.; Takeuchi, S.; Tsudzuki, S.; Miyatake, T.; Tanikaga, R. *Tetrahedron* **1998**, *54*, 6699–6718. (f) Kunieda, M.; Tamiaki, H. *J. Org. Chem.* **2008**, *73*, 7686–7694.

(17) (a) Huber, V.; Katterle, M.; Lysetska, M.; Würthner, F. *Angew. Chem., Int. Ed.* **2005**, *44*, 3147–3151. (b) Huber, V.; Lysetska, M.; Würthner, F. *Small* **2007**, *3*, 1007–1014. (c) Huber, V.; Sengupta, S.; Würthner, F. *Chem.—Eur. J.* **2008**, *14*, 7791–7807. (d) Ganapathy, S.; Sengupta, S.; Wawrzyniak, P. K.; Huber, V.; Buda, F.; Baumeister, U.; Würthner, F.; de Groot, H. J. M. *Proc. Natl. Acad. Sci. U.S.A.* **2009**, *106*, 11472–11477.

(18) (a) Tamiaki, H.; Kimura, S.; Kimura, T. *Tetrahedron* **2003**, *59*, 7423–7435. (b) Kunieda, M.; Tamiaki, H. *J. Org. Chem.* **2005**, *70*, 820–828. (c) Kunieda, M.; Tamiaki, H. *J. Org. Chem.* **2007**, *72*, 2443–2451. (d) Miyatake, T.; Tanigawa, S.; Kato, S.; Tamiaki, H. *Tetrahedron Lett.* **2007**, *48*, 2251–2254. (e) Tamiaki, H.; Nishiyama, T.; Shibata, R. *Bioorg. Med. Chem. Lett.* **2007**, *17*, 1920–1923. (f) Kunieda, M.; Tamiaki, H. *J. Org. Chem.* **2009**, *74*, 5803–5809.

(19) Balaban, T. S.; Bhise, A. D.; Fischer, M.; Linke-Schaetzel, M.; Roussel, C.; Vanthuyne, N. *Angew. Chem., Int. Ed.* **2003**, *42*, 2139–2144.

(20) Balaban, T. S.; et al. *J. Am. Chem. Soc.* **2009**, *131*, 14480–14492.

(21) Bhise, A. D. A biomimetic approach for synthesizing artificial light-harvesting systems using self-assembly. Ph.D. Thesis, Wissenschaftliche Berichte FZKA 7174, Universität Karlsruhe (TH), 2005; ISSN 0947-8620.

(22) Marquardt, C. W.; Blatt, S.; Hennrich, F.; von Löhneysen, H.; Krupke, R. *Appl. Phys. Lett.* **2006**, *89*, 183177.

(23) (a) Schenning, A. P. H. J.; Benneker, F. B. G.; Geurts, H. P. M; Liu, X. Y.; Nolte, R. J. M. *J. Am. Chem. Soc.* **1996**, *118*, 8549–8552. (b) Lensen, M. C.; Takazawa, K.; Elemans, J. A. A. W.; Jeukens, C. R. L. P. N; Christianen, P. C. M.; Maan, J. C.; Rowan, A. E.; Nolte, R. J. M. *Chem.—Eur. J.* **2004**, *10*, 831–839.

(24) (a) Mishra, A.; Behera, R. K.; Behera, P. K.; Mishra, B. K.; Behera, G. B. *Chem. Rev.* **2000**, *100*, 1973–2011. (b) Würthner, F.; Kaiser, T. E.; Saha-Möller, C. R. *Angew. Chem., Int. Ed.* **2011**, *50*, 3376–3410.

(25) Gorjanacz, M.; Török, I.; Pomozi, I.; Garab, G.; Szlanka, T.; Kiss, I.; Mechler, B. M. *J. Struct. Biol.* **2006**, *154*, 27–41.

(26) Steinbach, G.; Pomozi, I.; Zsiros, O.; Pay, A.; Horvath, G. V.; Garab, G. *Cytometry* **2008**, *73A*, 202–208.

(27) Kitahama, Y.; Kimura, Y.; Takazawa, K. *Langmuir* **2006**, *22*, 7600–7604.

(28) (a) Shibata, Y.; Saga, Y.; Tamiaki, H. *Photosynth. Res.* **2009**, *100*, 67–78. (b) Tamiaki, H.; Tateishi, S.; Nakabayashi, S.; Shibata, Y.; Itoh, S. *Chem. Phys. Lett.* **2010**, *484*, 333–337.

(29) (a) Furumaki, S.; Vacha, F.; Habuchi, S.; Tsukatani, Y.; Bryant, D. A.; Vacha, M. *J. Am. Chem. Soc.* **2011**, *133*, 6703–6710. (b) Furumaki, S.; Habuchi, S.; Vacha, M. *Chem. Phys. Lett.* **2010**, *487*, 312–314.

(30) Nilsson, J.; Evander, M.; Hammarström, B.; Laurell, T. *Anal. Chim. Acta* **2009**, *649*, 141–157.

(31) Ribó, J. M.; Crusats, J.; Sagues, F.; Claret, J. M.; Rubires, R. *Science* **2001**, *292*, 2063–2066.

(32) Escudero, C.; Crusats, J.; Diez-Perez, I.; El-Hachemi, Z.; Ribó, J. M. *Angew. Chem., Int. Ed.* **2006**, *45*, 8032–8035.

(33) El-Hachemi, Z.; Arteaga, O.; Crusats, J.; Escudero, C. E.; Kuroda, R.; Harada, T.; Rosa, M.; Ribó, J. M. *Chem.—Eur. J.* **2008**, *14*, 6438–6443.

(34) El-Hachemi, Z.; Mancini, G.; Ribó, J. M.; Sorrenti, A. *New J. Chem.* **2010**, *34*, 260–266.

(35) (a) Crusats, J.; El-Hachemi, Z.; Ribó, J. M. *Chem. Soc. Rev.* **2010**, *39*, 569–577. (b) Arteaga, O.; Canillas, A.; Crusats, J.; El-Hachemi, Z.; Llorens, J.; Ribó, J. M. *ChemPhysChem* **2010**, *11*, 3511–3516. (c) El-Hachemi, Z.; Arteaga, O.; Canillas, A.; Crusats, J.; Llorens, J.; Ribó, J. M. *Chirality* **2011**, *23*, 585–592.

(36) D'Urso, A.; Randazzo, R.; Lo Faro, L.; Purrello, R. *Angew. Chem., Int. Ed.* **2010**, *49*, 108–112.
(37) Tsuda, A.; Alam, Md. A.; Harada, T.; Yamaguchi, T.; Ishii, N.; Aida, T. *Angew. Chem., Int. Ed.* **2007**, *46*, 8198–8202.
(38) Balaban, T. S.; Leitich, J.; Holzwarth, A. R.; Schaffner, K. *J. Phys. Chem. B* **2000**, *104*, 1362–1372.
(39) Asano, N.; Harada, T.; Sato, T.; Tajima, N.; Kuroda, R. *Chem. Commun.* **2009**, 899–901.
(40) Balaban, T. S. In *Handbook of Porphyrin Science with Applications to Chemistry, Physics, Materials Science, Engineering, Biology and Medicine*; Kadish, K. M., Smith, K. M., Guilard, R., Eds.; World Scientific: Singapore, 2010; Vol. 1, pp 221−306.
(41) Ptaszek, M.; Yao, Z.; Savithri, D.; Boyle, P. D.; Lindsey, J. S. *Tetrahedron* **2007**, *63*, 12629–12638.
(42) Pšenčik, J.; Ikonen, T. P.; Laurinmäki, P.; Merckel, M. C.; Butcher, S. J.; Serimaa, R. E.; Tuma, R. *Biophys. J.* **2004**, *87*, 1165–1172.
(43) Balaban, T. S.; Fromme, P.; Holzwarth, A. R.; Krauss, N.; Prokhorenko, V. I. *Biochim. Biophys. Acta (Bioenergetics)* **2002**, *1556*, 197–207.
(44) Oba, T.; Tamiaki, H. *Photosynth. Res.* **2002**, *74*, 1–10.
(45) Oba, T.; Tamiaki, H. *J. Photosci.* **2002**, *9*, 362–363.
(46) (a) Balaban, T. S. *FEBS Lett.* **2003**, *545*, 97–102. Erratum: **2003**, *547*, 235. (b) Balaban, T. S. *Photosynth. Res.* **2005**, *86*, 251–262.
(47) Oba, T.; Tamiaki, H. *Bioorg. Med. Chem.* **2005**, *13*, 5733–5739.
(48) (a) Ashkin, A. *Proc. Natl. Acad. Sci. U.S.A.* **1997**, *94*, 4853–4860. (b) Gauthier, R. C.; Ashman, M.; Grover, C. P. *Appl. Opt.* **1999**, *38*, 4861–4869.
(49) Eisele, D. M.; Knoester, J.; Kirstein, S.; Rabe, J. P.; Van den Bout, D. A. *Nature Nanotechnol.* **2009**, *4*, 658–663.
(50) Pagola, S.; Stephens, P. W.; Bohle, S. D.; Kosar, A. D.; Madsen, S. K. *Nature* **2000**, *404*, 307–310.
(51) Oliveira, M. F.; Kycia, S. W.; Gomez, A.; Kosar, A. J.; Bohle, D. S.; Hempelmann, E.; Menezes, D.; Vannier-Santos, M. A.; Oliviera, P. L.; Ferreira, S. T. *FEBS Lett.* **2005**, *579*, 6010–6016.
(52) Garab, G.; Kiss, J. G.; Mustrardy, L. A.; Michel-Villaz, M. *Biophys. J.* **1981**, *34*, 423–437.
(53) Marek, P. L.; Hahn, H.; Balaban, T. S. *Energ. Environ. Sci.* **2011**, *4*, 2366–2378.
(54) Bürck, J.; Roth, S.; Wadhwani, P.; Afonin, S.; Kanithasen, N.; Standberg, E.; Ulrich, A. S. *Biophys. J.* **2007**, *95*, 3872–3881.